Journal of Materials Chemistry C

ROYAL SOCIETY OF CHEMISTRY

PAPER

View Article Online
View Journal

Cite this: DOI: 10.1039/d5tc04056f

Orientation control of $Cu_3(HHTP)_2$ MOF films using a dual working electrode electrochemical synthesis method

Yu Wang, Abigail M. Lister, Christopher E. Patrick, Sparsh Tyagi, Shengming Zhang, Axel Forssberg, Neil Young, Weishuo Li and Martin R. Castell *

Materials that consist of stacked two-dimensional electronically conductive metal–organic frameworks (2D-cMOFs) have potential for integration into novel electronic devices. These layered materials have crystal structures and charge transport properties that are highly anisotropic. For effective use as functional device materials it is therefore important to achieve control over the crystallographic orientation of the films and their growth mechanisms. Here we report an electrochemical method to synthesise $Cu_3(HHTP)_2$ films *in situ* on ITO glass with controllable film orientation and thickness using a dual working electrode setup. By adjusting the ligand concentration in the electrolyte, different $Cu_n(HHTP)_m$ complexes form, which interact differently with the electrode upon which the MOF is grown. This leads to the consistent formation of edge-on or face-on oriented MOF films. For high ligand concentrations the 2D layers grow perpendicular to the electrode substrate, whereas for low ligand concentrations the layers are parallel to the substrate. Extensive characterisation and theoretical simulations of this material system lead to the conclusion that growth of the different MOF orientations is a result of the electric dipoles on the $Cu_n(HHTP)_m$ complexes. Cu(HHTP) and $Cu_2(HHTP)$ complexes are created under high ligand concentration conditions and have electric dipoles that result in edge-on nucleation due to electrostatic interactions with the potential on the electrode. Under low ligand concentrations $Cu_3(HHTP)$ complexes are formed that do not have a dipole and nucleate face-on *via* van der Waals interactions.

Received 14th November 2025,
Accepted 22nd February 2026

DOI: 10.1039/d5tc04056f

rsc.li/materials-c

1. Introduction

Electrically conductive two-dimensional metal–organic frameworks (2D MOFs) are an evolving class of materials with potential for use in a variety of electronic devices such as chemiresistive sensors, field-effect transistors, and thermoelectric devices.[1,2] Achieving precise control over the morphology, contact resistance, thickness, and orientation of 2D MOF films is important for the optimisation of the performance of these devices. The thin film form factor is required to maximize surface-interaction-driven functionality for sensors, and enable reliable device operation for transistors.[3] Orientation control during materials integration into the device is especially relevant for stacked crystalline 2D MOF materials, where both structure and electrical conductivity are highly anisotropic.[4–6]

Various synthesis methods, such as layer-by-layer methods, vapor-assisted synthesis, electrochemical growth, and chemical vapor deposition have been developed to fabricate large area 2D MOF thin films.[7–13] Some of these methods have successfully achieved face-on oriented 2D MOF films where the 2D layers are parallel to the substrate surface. However, consistent fabrication of edge-on films, where the 2D layers are perpendicular to the substrate, remains challenging.[5,14,15] One effective strategy for achieving edge-on orientated films is to use the hydrophilic functional group of the ligand to induce the ligand to stand upright on the surface of –OH functionalized substrates and use layer-by-layer deposition to grow the films.[4,5,16] This method enables the fabrication of nanoscale-thickness films, however producing dense thicker films remain challenging due to the method's spraying process, which requires highly accurate repetitive operations. An alternative method for fabricating 2D MOF films is electrochemical synthesis.[17] This method has the advantages of high efficiency, relatively simple operation, scalability, and for enabling the control of film morphology and thickness.[10,14,18] Recently, a catalyst-assisted approach was introduced to controllably synthesize both face-on and edge-on oriented $Cu_3(HHTP)_2$ films by applying catalyst layers to modulate ligand oxidation kinetics.[19] This method requires catalytically active substrates and additional fabrication steps, which limits its direct applicability in the context of device integration.

Department of Materials, University of Oxford, Parks Road, Oxford OX1 3PH, UK. E-mail: martin.castell@materials.ox.ac.uk

The MOF synthesis method described here, enables orientation control of $Cu_3(HHTP)_2$ films through a catalyst-free electrochemical route by modulating the ligand concentration in solution. We grow edge-on and face-on oriented $Cu_3(HHTP)_2$ films on indium-doped tin oxide (ITO) substrates with controllable film orientation and thickness. This is achieved using a dual working electrode setup that enables the MOF formation and anodic oxidation of Cu to occur on separate surfaces. We also elucidate the growth mechanism responsible for the orientation control.[16,20] Our strategy provides flexibility in synthesis, broad compatibility with device substrates, and a mechanistic basis for tuning film orientation, offering a scalable route to high-quality, oriented 2D MOF films.

2. Experimental and theoretical techniques

2.1. Materials

2,3,6,7,10,11-Hexahydroxytriphenylene (HHTP) was purchased from Fluorochem Ltd, UK. Before use, the HHTP powder was dissolved in methanol, filtered through a sterile syringe filter with a 450 nm pore size, and subsequently dried under argon flow. Tributyl methyl ammonium methyl sulfate (TBMAMS) was purchased from Santa Cruz Biotechnology, USA. 3M copper tape (1181 series) with an acrylic adhesive was purchased from RS Components, UK. The copper tape was ground with an abrasive disk, and rinsed with water and ethanol before use. ITO-coated glass slides with a surface resistivity of 8–12 Ω sq^{-1} were purchased from Sigma Aldrich, UK. Before use, the ITO glass substrates were sonicated with DI water, acetone, and ethanol for 10 min each and then dried in air. No additional surface treatment was applied.

2.2. Synthesis methods

Solvothermal synthesis of $Cu_3(HHTP)_2$ powder was carried out using the following method. A solid mixture of HHTP (7.5 mg) and copper(II) acetate (10.5 mg) was suspended in 2 mL of deionized water in a glass vial. The vial was then sonicated for 10 min. The mixture was heated at 85 °C for 72 h resulting in dark blue crystals. The resulting powder was washed with deionized water, ethanol, and acetone three times and dried in air overnight.

Cyclic voltammetry (CV) was performed using a three-electrode set-up, with a Pt counter electrode and an Ag/AgCl reference electrode. For the HHTP CV measurement, the electrolyte solution contained 2.6 mM HHTP and 0.02 M TBMAMS in a 4 : 1 water and ethanol mixture, with ITO glass serving as the working electrode. In the case of the Cu tape measurement, the electrolyte solution contained 0.02 M TBMAMS in the same 4 : 1 water and ethanol mixture, with Cu tape used as the working electrode.

The same CV set-up was used for electrochemical synthesis of the $Cu_3(HHTP)_2$ oriented films on ITO as shown schematically in Fig. 1. Cu tape was adhered on the opposite side of the ITO glass, with the same size as the ITO substrate. We refer to this setup as a dual working electrode because the electrode is formed from two separate active surfaces. Different concentrations of ligand were employed in the synthesis of the oriented films. For the edge-on films, 2.6 mM HHTP powder and 0.02 M TBMAMS were dispersed in a mixed solution of 4 : 1 water and ethanol. For the face-on films, 1.3 mM HHTP powder and 0.02 M TBMAMS were dispersed in mixed solution of 4 : 1 water and ethanol. The solution was sonicated for 5 min before synthesis. The deposition was conducted for various times from 2 h to 10 h. The final film on ITO glass was washed using acetone.

2.3. Characterization

Scanning electron microscope (SEM) images were obtained using a Zeiss Merlin SEM. Samples for transmission electron microscopy (TEM) were dispersed in ethanol, and drop-cast onto a carbon coated copper grid. TEM images were obtained using a JEOL-2100 microscope at 200 kV. Powder X-ray diffraction (XRD) measurements were performed on a Rigaku Miniflex XRD with a 1.54 Å Cu Kα X-ray source. Film XRD measurements were performed on an Empyrean XRD. UV-vis absorption spectra were measured by using a Varian Cary 5000 UV-visible-NIR spectrometer. A Bruker Dimension Icon atomic force microscope (AFM) was used to characterise all samples in a glovebox filled with argon ($<$0.1 ppm H_2O, $<$0.1 ppm O_2) at room temperature. All AFM probes (SCM-PIT-V2) were calibrated according to standard samples (sapphire and Ti roughness sample) interpolating the actual spring constant and tip radius ($\sim$5 nm). The PeakForce Tunneling AFM (TUNA) method was conducted to capture both the topography of the samples and the corresponding TUNA current data (average current during a full tapping cycle). 3D topography images were reconstructed using NanoScope Analysis 2.0 software. The film thickness data were obtained from the height difference between the plated samples and the substrates. The current value used to calculate the resistance was the average TUNA current response in a field of view of 5 μm × 5 μm under different applied voltages between the AFM tip and the sample. The gradient of I *vs.* V was extracted by linear fitting to calculate the resistance, $R = (I/V)^{-1}$. With additional information of tip radius and thickness of the plated sample, the conductivity σ (S cm^{-1}) was calculated with the following formula,[16] where d (cm) is the film thickness, A (cm^2) is the tip area, $R(\Omega)$ is the resistance: $\sigma = d/(R \times A)$. X-ray photoelectron spectroscopy (XPS) was performed on a PHI VersaProbe III with a monochromatic Al Kα X-ray source (1486.6 eV).

2.4. Theoretical modelling

The electric dipole moments of the model complexes, discussed in Section 3.3, were calculated using density-functional theory (DFT), using plane wave basis sets and ultrasoft pseudopotentials as implemented in the Quantum ESPRESSO software package.[21–23] The complexes were placed in a cubic simulation cell of side length 20 Å and allowed to relax until the force on each atom was smaller than 26 meV $Å^{-1}$. The relaxed positions $\overrightarrow{R_I}$ and the electronic charge density $n(\vec{r})$ were then used to calculate the

electric dipole moment $\vec{p}$, as

$$\vec{p} = e \times \left[\sum_I Z_I \overrightarrow{R_I} - \int \vec{r} n(\vec{r}) \mathrm{d}\vec{r} \right]$$

where e is the electronic charge, and Z_I is the valence charge of the atom located at position $\overrightarrow{R_I}$. In the structural relaxations, exchange and correlation were treated within the generalized-gradient approximation using the PBE functional.[24] In order to evaluate the sensitivity of the electric dipole moments to the treatment of exchange and correlation, calculations were carried out both with the standard PBE functional and also with the hybrid PBE0 functional.[25] The PBE0 functional is more computationally expensive, but expected to be more accurate due to its inclusion of exact Hartree–Fock exchange. The same qualitative results were found with both functionals, with the dipoles of the complexes found to be 1.25 eÅ and 0.26 eÅ within PBE, and 1.46 eÅ and 0.10 eÅ within PBE0.

3. Results and discussion

3.1. Electrochemical MOF synthesis using a dual-working-electrode setup

As illustrated in Fig. 1a, we used a dual-working-electrode design where the working electrode is composed of copper tape adhered to the opposite side of an ITO substrate. The copper side of the working electrode acts as the Cu ion source, and the ITO side is where the oriented MOF grows. The electrolyte solution contains HHTP and TBMAMS in a mixed solvent of water/ethanol (v/v, 4 : 1). MOF formation requires an appropriate voltage to ionize the Cu and oxidize the ligand on the ITO electrode. The electrochemical behaviour of Cu and HHTP was investigated using cyclic voltammetry (CV) to determine the appropriate potential for electrochemical deposition. Previous studies have reported six one-electron-oxidation processes for HHTP after deprotonation, from fully reduced $HHTP^{6-}$ to fully oxidized $HHTP^{0}$.[26,27] As the CV scans in Fig. 2a show, the HHTP solution shows three anodic peaks at 0.43 V, 0.65 V, and 0.9 V, which are attributed to three one-electron-oxidation processes of HHTP from CatCatCat sequentially to CatCatSq, CatSqSq, and SqSqSq (Fig. 2b).[14,28,29] The ionization of the Cu tape starts at around 0.2 V and shows a peak around 0.43 V, indicating the oxidation of Cu in this potential window.[18] Following the CV scans we selected a potential of 0.43 V for our subsequent electrochemical MOF growth, which is the minimum potential that enables oxidation of both the Cu and the ligand. We ran the electrochemical cell for 1 hour at 0.43 V, following which a dark film was observed to have grown on both the Cu side and the ITO side of the working electrode.

We then investigated the black film that had grown on the ITO side of the working electrode to confirm that it is the expected $Cu_3(HHTP)_2$ MOF. The powder was scraped off for PXRD characterization. As shown in Fig. 3a, peaks at 4.9°, 9.6°, 12.6°, 16.6° and a double peak at 28.2°/28.55° correspond to the (100), (200), (210), (220) and (001) planes of $Cu_3(HHTP)_2$, respectively.[9] The XRD scan of the electrochemically synthesized $Cu_3(HHTP)_2$ powder (Fig. 3a, blue) is consistent with both the solvent synthesized $Cu_3(HHTP)_2$ powder (Fig. 3a, grey) and the XRD data reported in the literature.[9,10] Detailed insight into the electrochemically synthesized $Cu_3(HHTP)_2$ was also obtained using high resolution TEM analysis. The TEM images show two distinct types of ordered image. The image showing layers (Fig. 3b) is of the MOF in the orientation when viewed perpendicular to the *c*-axis *i.e.* along the MOF planes. The layer periodicity is measured to be 0.33 nm which corresponds to the (001) reflection in the XRD pattern (0.32 nm periodicity). The hexagonal structure shown in Fig. 3c is of the MOF viewed parallel to the *c*-axis *i.e.* perpendicular to the direction of the image in Fig. 3b showing the lattice structure of $Cu_3(HHTP)_2$.[30] The FFT pattern in the inset of Fig. 3c shows bright spots indicating periodicities ranging between 1.75 nm and 2.03 nm, corresponding to the 4.9° (100) reflection in the XRD pattern that has a 1.80 nm periodicity. The XRD and TEM results confirm the successful synthesis of $Cu_3(HHTP)_2$ on the ITO surface using our dual-working-electrode strategy.

3.2. Orientation control of the MOF

Having confirmed the successful formation of $Cu_3(HHTP)_2$ using the dual-working-electrode electrochemical synthesis

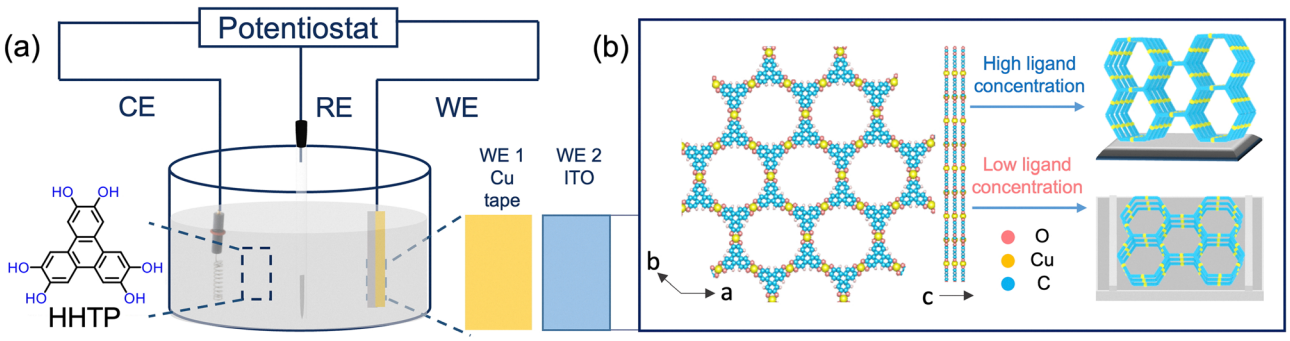

Fig. 1 Schematic illustration of the electrochemical synthesis setup for $Cu_3(HHTP)_2$ film deposition. The Cu tape serves as working electrode 1 (WE 1) and is adhered to the opposite side of the ITO, which acts as working electrode two (WE 2). A Pt electrode is used as counter electrode (CE), and Ag/AgCl as the reference electrode (RE). The HHTP ligand and TBMAMS electrolyte are dissolved in a water–ethanol mixture, which serves as the supporting electrolyte solution. (b) Structural models of $Cu_3(HHTP)_2$ are shown in both top and side views, along with schematic illustrations showing edge-on and face-on orientations with respect to the ITO substrate.

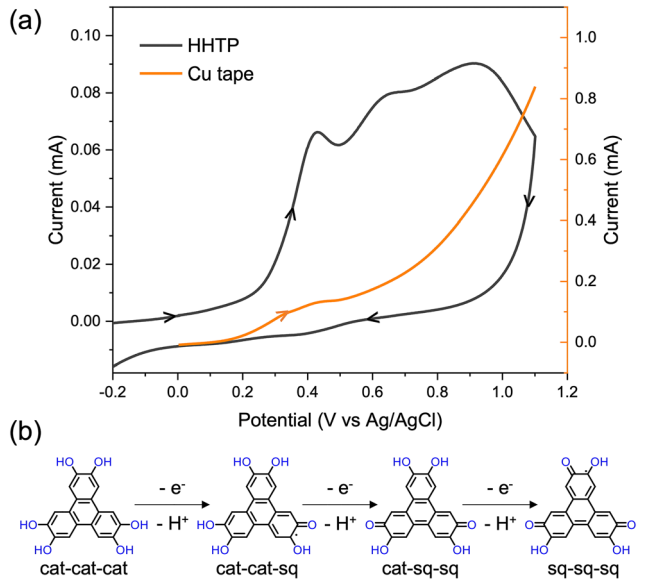

Fig. 2 (a) CV curves of HHTP solution (grey) and Cu tape (orange) measured on ITO glass at scan rates of 100 mV s^{-1}, with the scan initiated at 0 V in the positive direction. (b) Schematic illustration of the redox sequence of HHTP in the absence of metal ions and base, showing the oxidation from the H_6-HHTP (cat–cat–cat) to the H_3-HHTP$^{\bullet}$ (sq–sq–sq) state.

method described above, we varied the ligand concentration in the solution and found that this gives rise to distinct differences in the orientation and morphology of the MOF film on the ITO substrate. We applied the same 0.43 V potential to the working electrode throughout our experiments to ensure consistency. The SEM images of $Cu_3(HHTP)_2$ synthesized from a relatively high ligand concentration (2.6 mM HHTP powder in solution) show vertically oriented edge-on crystals (Fig. 4a) with their *c*-axis parallel to the ITO substrate surface. The $Cu_3(HHTP)_2$ film synthesized from a relatively low ligand concentration (1.3 mM HHTP powder in solution) forms face-on crystals with their *c*-axis perpendicular to the electrode surface (Fig. 4b).

PXRD measurements were performed to probe the stacking orientation of both the orientations of the $Cu_3(HHTP)_2$ MOF films. As shown in Fig. 5 (blue), the MOF film synthesized with a high ligand concentration exhibits strong diffraction peaks at 4.9°, 9.6°, 12.6°, and 16.6°, corresponding to the (100), (200), (210), and (220) planes, respectively. The presence of these peaks and the absence of a peak around 28° indicate edge-on orientation of the 2D layers *i.e.* the *c*-axes of the MOF crystals are parallel to the substrate surface.[4] In contrast, the film synthesized with a low ligand concentration has a strong double diffraction peak at 27.28° and 27.86° (Fig. 5 red), corresponding to interlayer stacking periodicities of 0.328 nm and 0.321 nm, repectively.[6] This double peak can be indexed to the (001) reflections of $Cu_3(HHTP)_2$, confirming the face-on orientation of the 2D layers. The two distinct *c*-axis periodicities correspond to coexisting slightly different planar stacking arrangements, previously reported as AA (or eclipsed) and AB (or near-eclipsed) stacking.[30,31] Our results confirm the formation of highly oriented and crystalline $Cu_3(HHTP)_2$ films using our electrochemical synthesis method, with a high ligand concentration promoting an edge-on orientation, and a low ligand concentration resulting in face-on stacking of $Cu_3(HHTP)_2$ layers.

XPS measurements were conducted to determine the oxidation state of the elements in the oriented $Cu_3(HHTP)_2$ films. As shown in Fig. S1a, the Cu spectrum shows a strong binding energy peak at 934.8 eV, corresponding to Cu^{2+}, along with a weak peak at 932.5 eV, suggesting the presence of Cu^{+}.[32] Both edge-on and face-on films show only low amounts of Cu^{+}, likely originating from structural defects, which indicate a well-coordinated crystalline structure.[33,34] The C 1s and O 1s spectra indicate the coexistence of C–O and C═O bonds, showing that catechol is partially oxidized to semiquinone in the HHTP ligand during coordination with Cu (Fig. S1b and c).[14,35] Our XPS results corroborate the XRD data to further demonstrate that we have grown highly crystalline films of $Cu_3(HHTP)_2$.

The growth of the oriented $Cu_3(HHTP)_2$ films was further investigated by varying the reaction times. In a solution with high ligand concentration, edge-on films with 2 h and 10 h reaction times are shown to have thicknesses of 0.56 μm and 2.5 μm, respectively (Fig. S2a and b). The MOF growth rate for the low ligand concentration solution was significantly faster, achieving 1.5 μm and 9.6 μm thicknesses over the same durations (Fig. S2c and d). As the reaction time is increased the roughness of the film also increases as shown in the AFM images in Fig. S2. It is interesting that the film synthesized from the low ligand concentration, which utilizes fewer reactants, exhibits more rapid growth compared with the film grown from a high ligand concentration. Presumably this is because the face-on orientation is smoother, enabling a $Cu_n(HHTP)_m$ molecule to land on the MOF surface and diffuse laterally to find an attachment site. This type of diffusion is inhibited for the edge-on orientation and this results in slower growth.

The local electrical conductivity of the films was determined through conductive AFM mapping (Fig. S3). This technique measures the local conductivity of the films with high spatial resolution.[16,36,37] The local average vertical conductivity through the edge-on film is $(6.78 \pm 0.45) \times 10^{-2}$ S cm^{-1} (Fig. S3e), while for the face-on film it is $(2.56 \pm 0.97) \times 10^{-5}$ S cm^{-1} (Fig. S3f). The in-plane charge transport is more than 10^3 times higher than the π–π stacking charge transport. These results are consistent with published transport properties in other MOFs where there is also a 2–3 orders of magnitude difference in the conductivity between the in-layer and across-layer orientations.[16] It should be noted that our absolute conductivity results are not as reliable as the relative conductivity ratio comparing face-on and edge-on films.

3.3. Growth mechanism of the oriented MOFs

The growth mechanism of the oriented films can be understood by examining the reactions and interactions occurring in solution and on the two sides (Cu tape and ITO slide) of the working electrode. The MOF growth mechanism on the copper

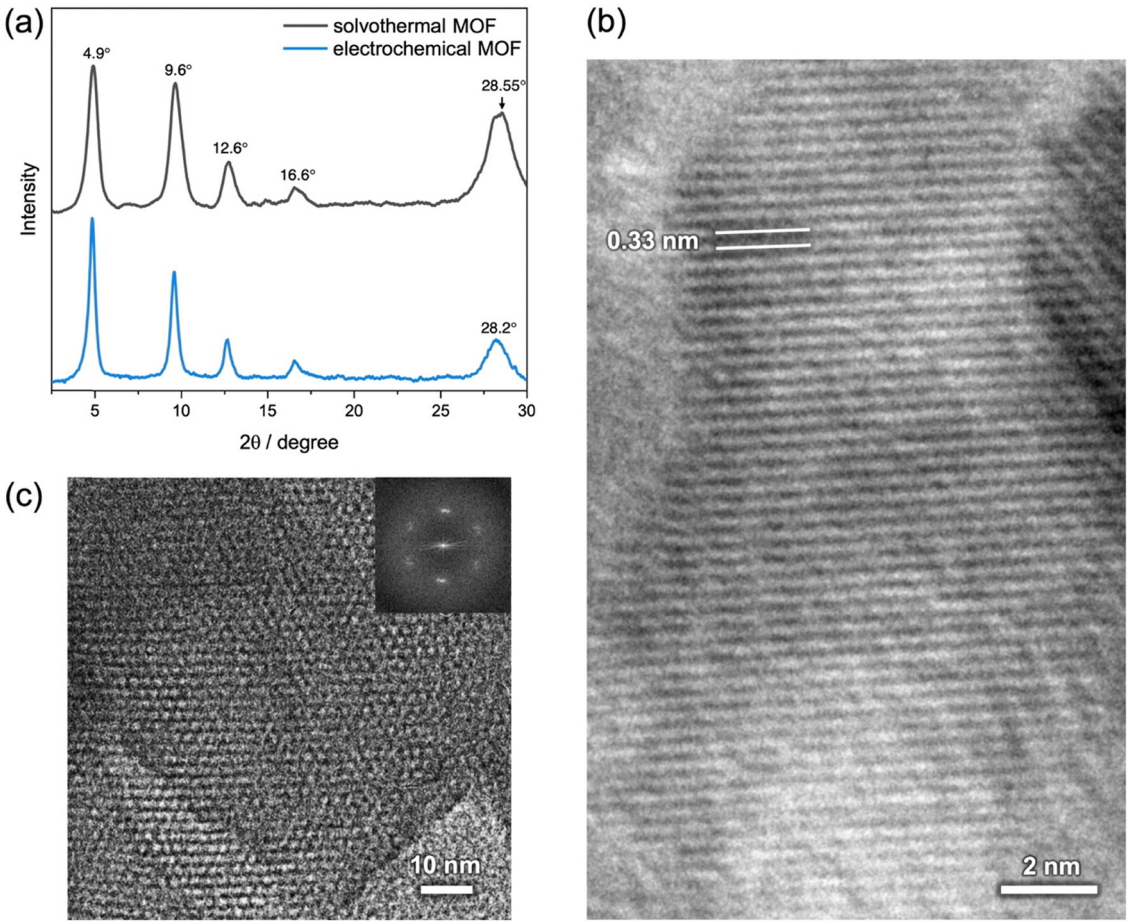

Fig. 3 (a) XRD pattern of solvothermally synthesized $Cu_3(HHTP)_2$ (grey) and electrochemically synthesized $Cu_3(HHTP)_2$ powder sample (blue), confirming the formation of $Cu_3(HHTP)_2$ using electrochemical synthesis. The high angle grey scan consists of a double peak at 28.2° and 28.55°, whereas the blue scan only has a single 28.2° peak. (b) HRTEM image of $Cu_3(HHTP)_2$ showing a measured interlayer distance of 0.33 nm. (c) HRTEM image of $Cu_3(HHTP)_2$. Inset: FFT pattern from the corresponding area showing the hexagonal structure of $Cu_3(HHTP)_2$.

side differs from that occurring on the ITO side. On the copper side, at the applied potential of +0.43 V, the Cu is ionised to Cu^{2+} and the HHTP is ionised from its catechol to semiquinone form. This enables $Cu_3(HHTP)_2$ MOF formation on the Cu tape through the coordination between the $(HHTP)^{3-}$ and Cu^{2+} ions. Face-on oriented films are grown on the Cu tape side of the working electrode no matter the ligand concentration, as shown in the SEM images in Fig. S4.

On the ITO side of the working electrode, no direct Cu source is available for MOF formation, and since the same voltage is applied to both the Cu tape and the ITO, there is no potential gradient between these two surfaces. For MOF growth to occur on the ITO electrode concentration-mediated Cu diffusion must occur to this electrode *via* either solvated Cu ions or $Cu_n(HHTP)_m$ complexes. Two experiments show that it is $Cu_n(HHTP)_m$ complexes that diffuse. The first experiment involves the preparation of separate solutions of $Cu(NO_3)_2$ and HHTP in a mixture of water and ethanol. When a drop of $Cu(NO_3)_2$ water:ethanol solution is added to an HHTP water:ethanol solution, an immediate blue colour change is observed. Since extended MOF formation is unlikely to occur this rapidly at room temperature without a base to facilitate deprotonation or higher temperatures to promote the reaction, the colour change suggests that intermediate $Cu_n(HHTP)_m$ complexes are formed. These complexes would also form in our solution for oriented growth following ionisation of the Cu electrode. This result further suggests that HHTP coordinates with a larger number of Cu ions in complexes formed under the low ligand concentration condition compared with the high ligand concentration.

The second experiment showing the existence of $Cu_n(HHTP)_m$ complexes involves UV-vis measurements. As shown in Fig. 6, the $Cu(NO_3)_2$ solution exhibits a light blue colour, with a broad peak at 810 nm. The ligand itself does not show any peaks in the metal–ligand charge transfer region. The MOF spectrum displays a broad absorption peak at about 664 nm, extending to the near-infrared (NIR) region, which can be attributed to the ligand-to-metal charge transfer transition (LMCT).[38,39] After 30 minutes of electrochemically-oriented MOF growth, a solution near the ITO surface was collected, both under high and low ligand concentration conditions. As shown in Fig. 6, the UV-vis spectra of the electrolyte solutions differ from those of HHTP, $Cu(NO_3)_2$, and

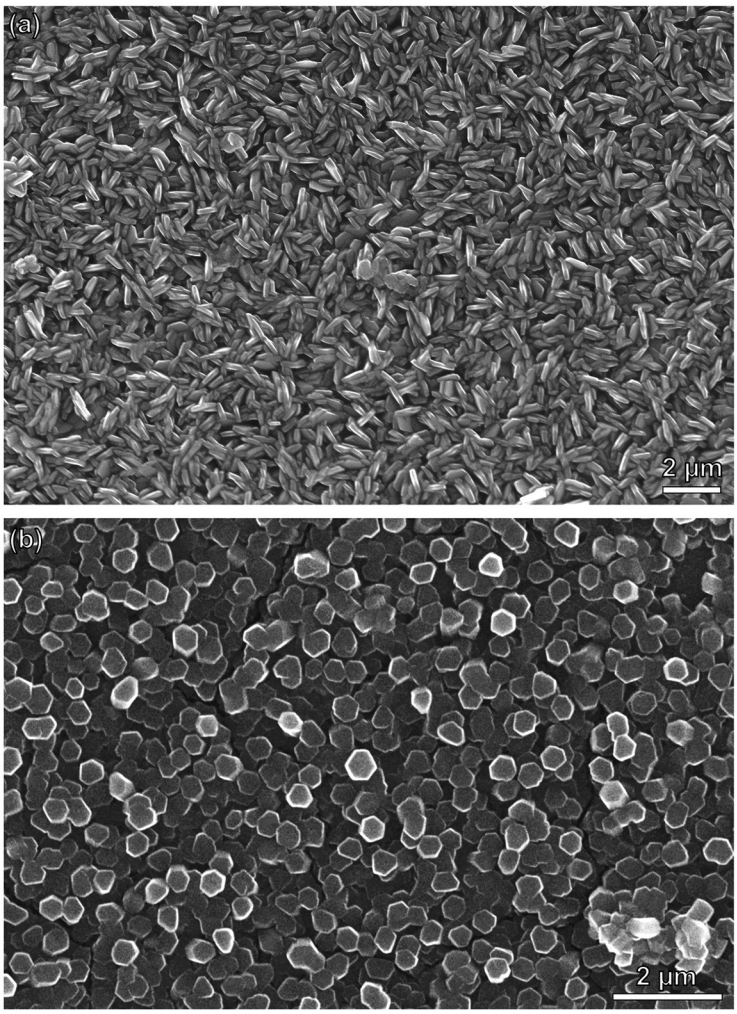

Fig. 4 SEM images of MOF crystals under different growth conditions. (a) Edge-on crystals grown under high ligand concentration conditions. (b) Face-on crystals grown under low ligand concentration conditions.

solvothermally synthesized $Cu_3(HHTP)_2$, confirming the presence of intermediate $Cu_n(HHTP)_m$ complexes. Compared to $Cu_3(HHTP)_2$ MOF, the complex formed in the high ligand concentration solution shows a blue shift in the LMCT band from 664 nm to 642 nm and a reduced NIR intensity. In contrast, the complexes formed in the low ligand concentration solution exhibit a red shift of the LMCT band shifting to 686 nm and an adsorption tail extending into the NIR region. The red shift of the LMCT band observed for complexes formed at low ligand concentration, relative to those formed at high ligand concentration, indicates an increased coordination number for the Cu ions.[40] The higher NIR to LMCT peak intensity ratio observed at low ligand concentration suggests more extensive metal–ligand charge transfer and greater conjugation within the resulting complexes.[41] Together, these results indicate that under low ligand concentration solution, HHTP coordinates with more Cu ions, resulting in larger complexes with higher Cu coordination number and increased electronic delocalization. The UV-vis results are compelling, but not definitive, because they do not provide direct structural information or coordination number. In addition, the low ligand concentration solution is a darker shade of blue than the high ligand concentration solution (Fig. S5). These results combined suggest that HHTP coordinates with a larger number of Cu ions in complexes formed under the low ligand concentration condition. Overall, the evidence indicates that Cu ions and HHTP molecules form different intermediate complexes under different ligand concentrations.

To gain further insight into the reaction occurring at the ITO side, we examined the importance of the applied voltage. A control experiment was performed where we applied the electrochemical potential only to the Cu surface, and left the ITO surface at ground potential. The formation of $Cu_3(HHTP)_2$ was observed on the Cu side, but not on the ITO side, indicating that a charged electrode surface is necessary for MOF growth on the ITO. The formation of MOF on the ITO electrode is therefore an electrochemically driven process between the $Cu_n(HHTP)_m$ complexes, solvated Cu ions, and HHTP ligands.

We now turn to the origin of the mechanism that results in orientated MOF growth. From the experiments reported above we know that $Cu_n(HHTP)_m$ complexes exist in the solution, and

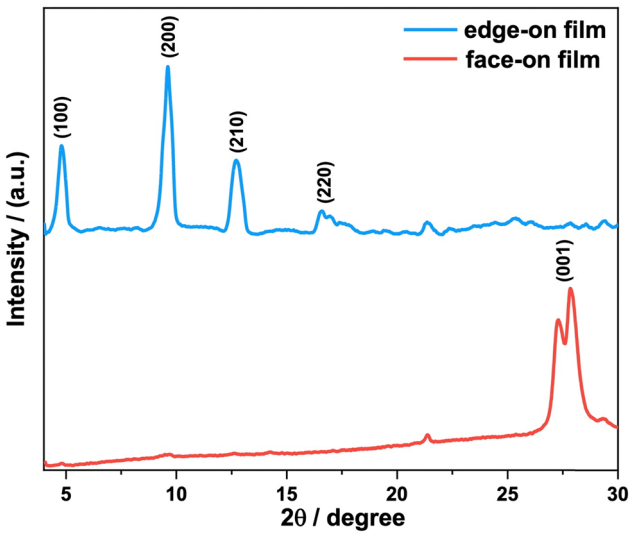

Fig. 5 PXRD scans of the oriented MOFs on ITO substrates. The edge-on orientation is shown in blue and the face-on orientation is shown in red. All the possible diffraction peaks are shown in blue apart from the (001) peak, which is the only one to appear in the face-on oriented film.

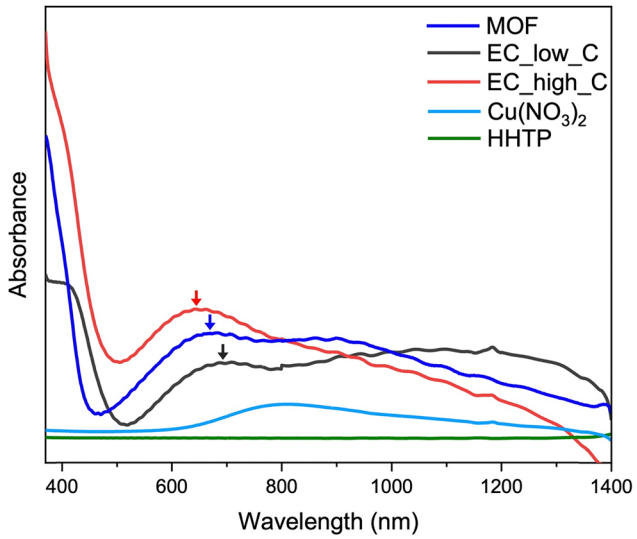

Fig. 6 UV-vis spectra of HHTP (green), $Cu(NO_3)_2$ (light blue), $Cu_3(HHTP)_2$ (blue), solution from high concentration electrochemical synthesis condition (red), and solution from low ligand concentration electrochemical synthesis condition (grey). The ligand-to-metal charge transfer transition peaks are indicated with arrows. The extended MOF peak (blue) is red-shifted for the high ligand concentration (red) and blue-shifted for the low ligand concentration (grey).

that these complexes have different colours and UV-vis signatures depending on the amount of ligand in the solution. The smallest complexes involve only one HHTP molecule with Cu ions bound to the dehydrogenated sites as shown in Fig. 7: Cu(HHTP), Cu_2(HHTP), and Cu_3(HHTP). We did not model higher $Cu_n(HHTP)_m$ complexes involving more than one HHTP molecule, although these are also likely to be present in the solution. As can be seen in the annotations in Fig. 7, there are in-plane electric dipole moments associated with the Cu(HHTP) and Cu_2(HHTP) molecules. The Cu(HHTP) dipole is particularly strong at 1.25 eÅ, and the Cu_2(HHTP) dipole is weaker at 0.26 eÅ. These dipole strengths can be compared with that of H_2O molecules, which in their liquid state is around 0.6 eÅ, and in the gas phase 0.38 eÅ.[42] The DFT calculations were performed using both the PBE and PBE0 functionals, and the same qualitative results were found. For HHTP coordinated with a single Cu ion, the electric dipole moment was 1.25 eÅ within PBE and 1.46 eÅ within PBE0. Coordination to two Cu atoms reduces the electric dipole moment to 0.26 eÅ within PBE and 0.1 eÅ within PBE0, while a fully coordinated HHTP shows no electric dipole moment. The out-of-plane electric dipole moment perpendicular to the Cu_nHHTP_m complex plane remains zero in all cases.

On diffusing to the ITO electrode, the Cu(HHTP) and Cu_2(HHTP) complex molecules will align their planar dipoles with the electric field that is created by the applied electrochemical potential. This will result in an edge-on orientation for the nucleating MOF film. Fully coordinated Cu_3(HHTP) molecules do not have a dipole associated with them and will therefore maximise their van der Waals interaction by attaching face-on to the ITO electrode resulting in a face-on nucleated MOF film. We reason that low ligand concentrations result in mainly fully-coordinated Cu_3(HHTP) molecules because all the solvated Cu ions can find an HHTP binding site. Conversely, for high ligand concentrations there are not sufficient numbers of Cu ions to fully coordinate all the ligand binding sites, and this results in undercoordinated Cu(HHTP) and Cu_2(HHTP) molecules with strong planar dipoles. The UV-vis spectra in Fig. 6 support this interpretation.

To investigate whether the formation of the oriented films is dominated by crystal nucleation or growth, we performed a control experiment by switching the synthesis conditions for edge-on and face-on films after 3 minutes of synthesis. ITO glass with Cu tape on the opposite side was submerged in an electrolyte solution with a high ligand concentration, and a voltage of 0.43 V was applied for 3 minutes. The combined working electrode was then transferred to a low ligand concentration solution. After 60 further minutes of synthesis, an edge-on film was observed. Conversely, when the electrode was initially placed in a low ligand concentration solution for 3 minutes under 0.43 V, and then transferred to the high ligand concentration condition, after 60 further minutes of synthesis, a face on film was observed. These results show that the film orientation is determined during the initial nucleation stage, and that once a film is oriented in a particular growth direction, then this orientation is maintained even if the growth conditions are subsequently changed to favour an alternative nucleation condition.

4. Conclusions

We have developed a dual-working electrode electrochemical synthesis method to fabricate $Cu_3(HHTP)_2$ films, enabling

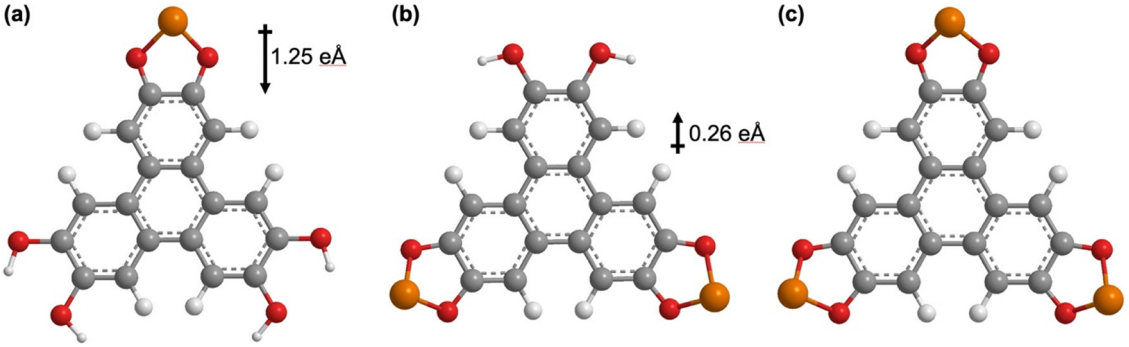

Fig. 7 (a) Cu(HHTP) molecule showing the DFT calculated dipole moment of 1.25 eÅ using a PBE functional. (b) Cu_2(HHTP) molecule with a 0.26 eÅ dipole. (c) The fully-coordinated Cu_3(HHTP) molecule does not have a dipole associated with it. Atom colours: C grey, O red, H white, Cu orange.

oriented MOF growth. This setup allows the oxidation of the metal and the MOF formation to occur at separate electrode surfaces, enabling highly crystalline and pure MOF films of varying thicknesses to be grown. By tuning the ligand concentration, well-oriented edge-on and face-on $Cu_3(HHTP)_2$ films were grown on an ITO electrode surface. Our investigation into the growth mechanism of oriented $Cu_3(HHTP)_2$ under different ligand concentration conditions emphasizes the importance of the intermediate $Cu_n(HHTP)_m$ complexes formed before MOF formation. The oriented edge-on film and face-on films exhibit anisotropic conductivity. The local conductivity along the in-plane direction was found $\sim 10^3$ times higher than across the planes.

This study presents a new strategy for electrochemical growth of oriented 2D MOF films on electrodes, providing a deeper understanding of their growth mechanisms. The results provide further opportunities for the design and synthesis of 2D MOF films with highly anisotropic charge transport properties. For device integration it may be necessary to tune the surface roughness of the films, which could be achieved through post-growth processing such as solvent vapour annealing[43] or plasma etching.[44]

Author contributions

M. R. C and Y. W. designed the research. Y. W. performed the synthesis and characterization. A. M. L assisted with MOF powder synthesis and data interpretation. C. E. P conducted the DFT simulations. S. T. and W. L. assisted with data interpretation and manuscript preparation. S. Z. performed the AFM experiment. A. F. conducted the XPS analysis. N. Y. performed TEM image capture and analysis.

Conflicts of interest

There are no conflicts to declare.

Data availability

The data that support the findings of this study are available in the supplementary information (SI) file and on request from the corresponding author. Supplementary information is available. See DOI: https://doi.org/10.1039/d5tc04056f.

Acknowledgements

We are grateful for computational support from the UK national high performance computing service, ARCHER2, for which access was obtained *via* the UKCP consortium and funded by EPSRC Grant ref EP/P022561/1.

References

1 L. S. Xie, G. Skorupskii and M. Dincă, *Chem. Rev.*, 2020, **120**, 8536–8580.
2 J. Liu, X. Song, T. Zhang, S. Liu, H. Wen and L. Chen, *Angew. Chem., Int. Ed.*, 2021, **60**, 5612–5624.
3 H. Jeong, G. Park, J. Jeon and S. S. Park, *Acc. Chem. Res.*, 2024, **57**, 2336–2346.
4 Z.-Z. Ma, Q.-H. Li, Z. Wang, Z.-G. Gu and J. Zhang, *Nat. Commun.*, 2022, **13**, 6347.
5 M.-S. Yao, K.-i Otake, T. Koganezawa, M. Ogasawara, H. Asakawa, M. Tsujimoto, Z.-Q. Xue, Y.-H. Li, N. C. Flanders and P. Wang, *Proc. Natl. Acad. Sci. U. S. A.*, 2023, **120**, e2305125120.
6 T. Hong, C. Lee, Y. Bak, G. Park, H. Lee, S. Kang, T. H. Bae, D. K. Yoon and J. G. Park, *Small*, 2024, **20**, 2309469.
7 J. Liu, Y. Chen, X. Huang, Y. Ren, M. Hambsch, D. Bodesheim, D. Pohl, X. Li, M. Deconinck and B. Zhang, *Nat. Synth.*, 2024, **3**, 715–726.
8 M. Choe, J. Y. Koo, I. Park, H. Ohtsu, J. H. Shim, H. C. Choi and S. S. Park, *J. Am. Chem. Soc.*, 2022, **144**, 16726–16731.
9 M. S. Yao, X. J. Lv, Z. H. Fu, W. H. Li, W. H. Deng, G. D. Wu and G. Xu, *Angew. Chem., Int. Ed.*, 2017, **56**, 16510–16514.
10 Y. Liu, Y. Wei, M. Liu, Y. Bai, X. Wang, S. Shang, J. Chen and Y. Liu, *Angew. Chem., Int. Ed.*, 2021, **60**, 2887–2891.
11 S. H. R. Shin, J. Tao, N. L. Canfield, M. E. Bowden, J. Heo, D. Li, J. Liu, J. J. De Yoreo, P. K. Thallapally and M. L. Sushko, *Adv. Mater. Interfaces*, 2023, **10**, 2202031.
12 R. M. Stolz, A. F. Kolln, B. C. Rocha, A. Brinks, A. M. Eagleton, L. Mendecki, H. Vashisth and K. A. Mirica, *ACS Nano*, 2022, **16**, 13869–13883.

13 A. M. Lister, Y. Wang, B. I. Armitage, W. Li and M. R. Castell, *J. Phys. Mater.*, 2025, **8**, 025004.
14 M. Song, J. Jia, P. Li, J. Peng, X. Pang, M. Qi, Y. Xu, L. Chen, L. Chi and G. Lu, *J. Am. Chem. Soc.*, 2023, **145**, 25570–25578.
15 A. Mähringer, A. C. Jakowetz, J. M. Rotter, B. J. Bohn, J. K. Stolarczyk, J. Feldmann, T. Bein and D. D. Medina, *ACS Nano*, 2019, **13**, 6711–6719.
16 Z. Wang, L. S. Walter, M. Wang, P. S. Petkov, B. Liang, H. Qi, N. N. Nguyen, M. Hambsch, H. Zhong and M. Wang, *J. Am. Chem. Soc.*, 2021, **143**, 13624–13632.
17 A. M. Lister, B. I. Armitage, Y. Wang, R. Chen, W. Li and M. R. Castell, *ACS Appl. Nano Mater.*, 2025, **8**, 15114–15121.
18 M. de Lourdes Gonzalez-Juarez, E. Flores, M. Martin-Gonzalez, I. Nandhakumar and D. Bradshaw, *J. Mater. Chem. A*, 2020, **8**, 13197–13206.
19 M. Song, Y. Wu, J. Jia, J. Peng, Y. Ren, J. Cheng, Y. Xu, W. Liu, S. Kang and Y. Fang, *J. Am. Chem. Soc.*, 2025, **147**, 17058–17067.
20 R. Zheng, Z.-H. Fu, W.-H. Deng, Y. Wen, A.-Q. Wu, X.-L. Ye and G. Xu, *Angew. Chem., Int. Ed.*, 2022, **61**, e202212797.
21 P. Giannozzi, S. Baroni, N. Bonini, M. Calandra, R. Car, C. Cavazzoni, D. Ceresoli, G. L. Chiarotti, M. Cococcioni and I. Dabo, *J. Phys.: Condens. Matter*, 2009, **21**, 395502.
22 D. Vanderbilt, *Phys. Rev. B: Condens. Matter Mater. Phys.*, 1990, **41**, 7892–7895.
23 A. Dal Corso, *Comput. Mater. Sci.*, 2014, **95**, 337–350.
24 J. P. Perdew, K. Burke and M. Ernzerhof, *Phys. Rev. Lett.*, 1996, **77**, 3865–3868.
25 C. Adamo and V. Barone, *J. Chem. Phys.*, 1999, **110**, 6158–6170.
26 C. S. Grange, A. J. Meijer and M. D. Ward, *Dalton Trans.*, 2010, **39**, 200–211.
27 L. Yang and M. Dincă, *Angew. Chem., Int. Ed.*, 2021, **60**, 23784–23789.
28 X. Du, J. Zhang, H. Wang, Z. Huang, A. Guo, L. Zhao, Y. Niu, X. Li, B. Wu and Y. Liu, *Mater. Chem. Front.*, 2020, **4**, 243–251.
29 K. P. Naidek, C. R. Zuconelli, O. M. Cruz, R. Ribeiro, S. M. Winnischofer and H. Winnischofer, *Biochem. Cell Biol.*, 2016, **94**, 205–211.
30 R. W. Day, D. K. Bediako, M. Rezaee, L. R. Parent, G. Skorupskii, M. Q. Arguilla, C. H. Hendon, I. Stassen, N. C. Gianneschi and P. Kim, *ACS Cent. Sci.*, 2019, **5**, 1959–1964.
31 J. W. Gittins, C. J. Balhatchet, S. M. Fairclough and A. C. Forse, *Chem. Sci.*, 2022, **13**, 9210–9219.
32 A. C. Gómez-Herrero, C. Sánchez-Sánchez, F. Chérioux, J. I. Martínez, J. Abad, L. Floreano, A. Verdini, A. Cossaro, E. Mazaleyrat and V. Guisset, *Chem. Sci.*, 2021, **12**, 2257–2267.
33 Y. Misumi, A. Yamaguchi, Z. Zhang, T. Matsushita, N. Wada, M. Tsuchiizu and K. Awaga, *J. Am. Chem. Soc.*, 2020, **142**, 16513–16517.
34 T. Chen, J.-H. Dou, L. Yang, C. Sun, N. J. Libretto, G. Skorupskii, J. T. Miller and M. Dincă, *J. Am. Chem. Soc.*, 2020, **142**, 12367–12373.
35 Y. Chen, Q. Zhu, K. Fan, Y. Gu, M. Sun, Z. Li, C. Zhang, Y. Wu, Q. Wang and S. Xu, *Angew. Chem., Int. Ed.*, 2021, **60**, 18769–18776.
36 F. Giannazzo, G. Greco, F. Roccaforte, C. Mahata and M. Lanza, *Electrical Atomic Force Microscopy for Nanoelectronics*, 2019.
37 E. Osuna, P. Ares, J. Gómez-Herrero, G. Llauradó-Capdevila, D. Rodríguez-San-Miguel, S. Pané, J. Puigmartí-Luis and C. Gómez-Navarro, *Small*, 2025, **21**, 2407945.
38 Q. Zuo, T. Liu, C. Chen, Y. Ji, X. Gong, Y. Mai and Y. Zhou, *Angew. Chem., Int. Ed.*, 2019, **58**, 10198–10203.
39 Y.-M. Jo, K. Lim, J. W. Yoon, Y. K. Jo, Y. K. Moon, H. W. Jang and J.-H. Lee, *ACS Cent. Sci.*, 2021, **7**, 1176–1182.
40 M. J. Sever and J. J. Wilker, *Dalton Trans.*, 2004, 1061–1072.
41 J. Wang, T. Chen, M. Jeon, J. J. Oppenheim, B. Tan, J. Kim and M. Dincă, *J. Am. Chem. Soc.*, 2024, 146, 20500–20507.
42 C. Adamo, M. Cossi, G. Scalmani and V. Barone, *Chem. Phys. Lett.*, 1999, **307**, 265–271.
43 S. Iwamoto, R. Nakayama, S. Chon, R. Shimizu and T. Hitosugi, *J. Mater. Chem. A*, 2024, **12**, 17492–17500.
44 P. V. Alekseevskiy, M. Timofeeva, S. Bachinin, R. Peignier, C. Noel, P. Boulet, T. Belmonte and V. A. Milichko, *Opt. Mater.*, 2024, **154**, 115666.